

Active sub-reflector research for a large radio telescope

Jin-Qing Wang, Rong-Bin Zhao, Yong-Chen Jiang, Zheng-Xiong Sun, Lin-Feng Yu, Li Fu, Qin-Hui Liu, Wei-Min Zheng and Zhi-Qiang Shen

Shanghai Astronomical Observatory, Chinese Academy of Sciences, Shanghai 200030, China; jqwang@shao.ac.cn
Key Laboratory of Radio Astronomy, Chinese Academy of Sciences, Nanjing 210008, China
Shanghai Key Laboratory of Space Navigation and Positioning Techniques, Shanghai 430074, China

Received 2019 May 8; accepted 2019 June 28

Abstract This paper proposes an active sub-reflector suitable for large radio telescopes, which can compensate both of the deformation of the main reflector and sub-reflector position offsets. The mathematical formula of the main reflector deformation compensated by the sub-reflector is deduced based on Cassegrain and Gregory antenna structures. The position of the sub-reflector is adjustable to compensate for defocusing errors on high and low elevations, which are mainly caused by the deformation of the sub-reflector supporting legs. In this paper, the method of obtaining the optimum position of the sub-reflector from the aperture phase by the interferometric method is introduced. The actual measurement is verified on the Tianma 65 m radio telescope, which provides a new way to diagnose the position error of the sub-reflector.

Key words: radio telescope — deformable sub-reflector — model — holography — phase

1 OVERVIEW

Mechanical and electronic compensation methods are commonly used to compensate the main reflector deformation of large radio telescopes (Wang & Li 2014). Mechanical compensation methods are divided into three types, which are active surface compensation (Nikolic et al. 2007), deformable beam-waveguide mirrors compensation (Hoppe 2001), and deformable sub-reflector compensation (Lawson & Yen 1988; Katow et al. 1983; Antebi et al. 1994; von Hoerner & Wong 1979). The earliest large radio telescope equipped with a deformable sub-reflector was the NRAO 140-foot radio telescope in Green Bank, United States. Due to the application of the deformable sub-reflector, the beam shape of this radio telescope was effectively improved and the ability to observe the water maser line at 22.3 GHz was significantly improved. However, this radio telescope has several drawbacks: (i) it only contains four actuators for the adjustment and the method is relatively simple; and (ii) it mainly takes into account of the “homology” error caused by deformation of the main reflector, the defocus problem, and the low-order components of deformation except the high-order error. To overcome these problems, the sub-surface divided in slices was proposed in von Hoerner & Wong (1979). As the observation frequency increases, different slice models have a great impact on the compensation performance.

In addition, the compensation of the sub-reflector in von Hoerner & Wong (1979) was derived from the known deformation of the main reflector by the ray tracing method. In 2006, a deformable sub-reflector was installed on the Bonn 100-meter radio telescope, which was an active sub-reflector controlled by 96 actuators to compensate for the gravity deformation of the main reflector. The aperture efficiency in high frequency was obviously improved after the simulation compensation model adopted. Where the main reflector shape error is known, the compensation model can be established for the deformable sub-reflector. The geometrical optical method can then be applied to calculate the deviation of the corresponding Cassegrain sub-reflector (Katow et al. 1983). As far as domestic research is concerned, the position adjustable sub-reflector has been widely investigated. However, the research of deformable sub-reflector is still in its initial stage. In Viskum & Klooster (2013), the main reflector matrix is constructed by sampling lines. Then, the compensation surface is designed by constraining the laws of reflection, energy conservation, and equal optical path.

The electronic compensation method of transmitting the compensation signal with a feed array was also adopted in application of large radio telescopes (Wu 2015; Xu et al. 2009). The phase of the signal transmitted by the feed array can be adjusted to compensate the deformation of the

main reflector. This method may cause additional noise injected. Therefore, this method may not be suitable for radio telescopes with very low noise.

Compared with the active main reflector, the deformable sub-reflector has several advantages: (i) the deformable sub-reflector is much more compact; (ii) the number of actuators is small; and (iii) it is very easy to control and the assembling cost is relatively low. The disadvantages are: (i) the resolution of the compensation may be coarse; (ii) the actuator and the panel division need to be arranged according to the deformation of the main reflector; and (iii) the shielding of the electromagnetic interference must be ensured in the engineering implementation.

The position adjustable sub-reflector can achieve effective focusing and improve the antenna efficiency degradation that is caused by the deformation of the sub-reflector's supporting legs, the back frame, and the main reflector on the high and low elevation. The Atacama Large millimeter/submillimeter Array (ALMA) (Gasho et al. 2003), The Submillimeter Array (SMA) (Cheimets 1994), Green Bank Telescope (GBT) and other international famous telescopes are equipped with such position adjustable sub-reflectors. For domestic radio telescopes, adjustable sub-reflectors have been installed on the Delingha 13.7 m millimeter wave telescope (Zuo et al. 2011), the Tianma 65 m (TM65) radio telescope, the Nanshan 26-meter radio telescope, and the deep-space station 66-meter antenna (Leng & Wang 2011). The achievements on 65 meters shows that below X -band, the 90% efficiency drop can be compensated by the sub-reflector position model in the entire elevation range (Wang et al. 2014). However, the reflector deformation compensation is necessary for frequencies higher than Ku -band.

This paper proposes an active sub-reflector based on both deformable reflector and adjustable position to improve the performance of large radio telescopes in all frequency bands and entire elevation range.

2 ACTIVE SUB-REFLECTOR

2.1 An Equal Optical Path Length Compensation Method for a Deformable Sub-reflector

The surface shape of the sub-reflector is deformable to compensate the deformation of the main reflector. This paper mainly analyzes two antenna structures — the Cassegrain and Gregory antenna structures. Using the method of ray tracing, these antenna structures are considered as two examples to introduce the method of compensating the main reflector deformation with the constant optical path length as the constraint. The parallel light emitted is divided into three segments for consideration. The first segment starts from the feed to the sub-reflector, the

second segment is from the sub-reflector to the main reflector, and the third segment is the main reflector to the aperture plane. Then, the difference between each optical path and the ideal optical path is calculated. Finally, these three optical path differences are accumulated. The correspondence between the main reflector deformation and the sub-reflector deformation is given in Table 1. It is noted that the constraint condition is that the reflected light is parallel to the incident light during the calculation.

Figure 1 shows the overall optical path of the Cassegrain antenna. The shape of the main reflector and sub-reflector is in red. The ideal optical path is in black along with the tangent line on the reflecting point that is in a black-dashed line. Now we suggest the deformation of the main reflector is Δ which caused the compensation of the sub-reflector is ε . The tangent lines are parallel to the original ones and the dashed lines are in green. Figure 2 shows the optical path variation dl_1 caused by the deformation of the sub-reflector along with the derivation formula of the optical path. Here we suggest the light start from the Cassegrain focus. l_1 is the ideal first path length from the focus to the sub-reflector. The θ and 2Φ are the angles between the original light and the axis, the reflected light and axis respectively. β is the angle of reflection at the sub-reflector. Now given an offset ε for the sub-reflector compensation and then we can derive the relationship between the change of l_1 and ε that is

$$dl_1 = -\frac{\varepsilon}{\cos\beta} = -\frac{\varepsilon}{\cos(\frac{2\phi+\theta}{2})}, \quad (1)$$

$$\beta = \frac{2\phi + \theta}{2}. \quad (2)$$

Figure 3 shows the optical path variation dl_2 caused by the deformation of the sub-reflector dl'_2 and main reflector dl''_2 . Here a is the gap between the original light and the changed from sub-reflector to the main reflector. At last we get

$$a = 2 \cdot \varepsilon \cdot \sin\left(\frac{2\phi + \theta}{2}\right), \quad (3)$$

$$dl'_2 = -dl_1 \cdot \cos(2\beta), \quad (4)$$

$$dl''_2 = \frac{\Delta}{\cos(\phi)} - a \cdot \tan(\phi), \quad (5)$$

$$\begin{aligned} dl_2 &= dl'_2 + dl''_2 \\ &= \frac{\varepsilon \cdot \cos(2\phi + \theta)}{\cos(\frac{2\phi+\theta}{2})} + \frac{\Delta}{\cos(\phi)} \\ &\quad - 2 \cdot \varepsilon \cdot \sin(\frac{2\phi + \theta}{2}) \cdot \tan(\theta). \end{aligned} \quad (6)$$

Figure 4 shows the optical path variation dl_3 from the main reflector to the aperture plane. Here the blue-dashed

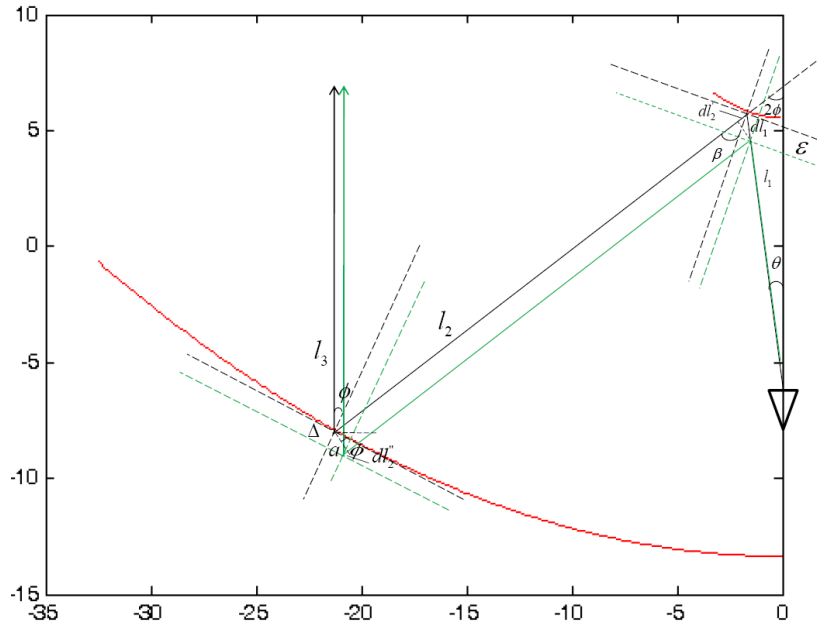


Fig. 1 Optical path of Cassegrain antenna.

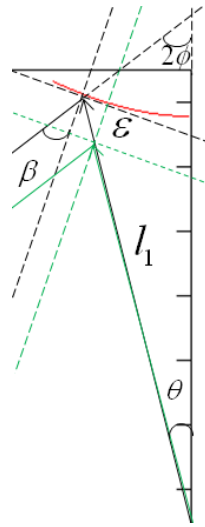


Fig. 2 The optical path variation dl_1 caused by the deformation of the sub-reflector.

line is from the reflection point on the main reflector and normal to the optical axis. We can get

$$dl_3 = \frac{a}{\sin(2\phi)} - x, \quad (7)$$

$$x = b \cdot \cos(2\phi), \quad (8)$$

$$b = \frac{a}{\sin(2\phi)} - \frac{\Delta}{\cos(\phi)}, \quad (9)$$

$$dl_3 = 2 \cdot \varepsilon \cdot \sin\left(\frac{2\phi + \theta}{2}\right) \cdot \tan(\phi) + \frac{\cos(2\phi)}{\cos(\phi)} \cdot \Delta. \quad (10)$$

The situation of the Gregory antenna is shown in Figure 5. The overall optical path changing is listed in Table 1.

To keep the optical path unchanged when the normal direction of the main reflector is adjusted to -3 mm, the compensation of the sub-reflector for the Cassegrain antenna is shown in Figure 6. It is shown that the compensation at the center of the sub-reflector is the same as that of the main reflector, and the area away from the center will compensate for the same deformation of the main reflector with a slightly larger amount of the sub-reflector

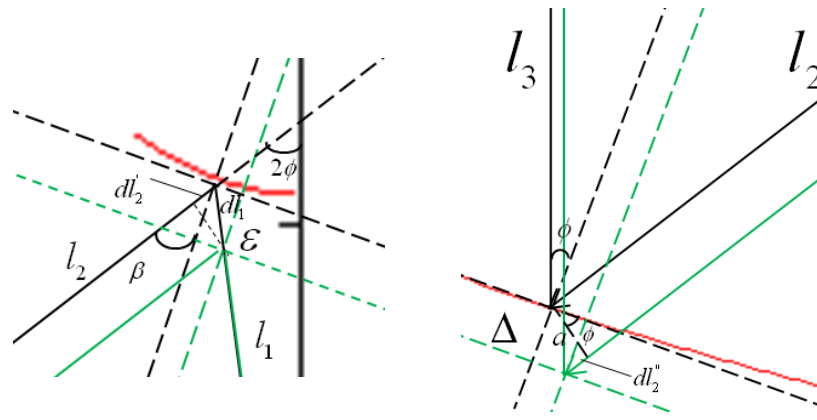


Fig. 3 The optical path variation dl_2 caused by the deformation of the sub-reflector and main reflector.

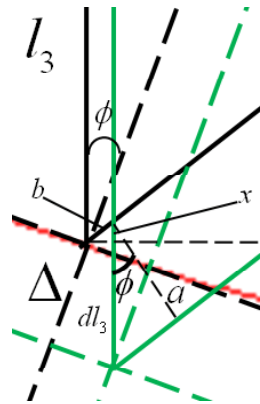


Fig. 4 The optical path variation dl_3 from the main reflector to the aperture plane.

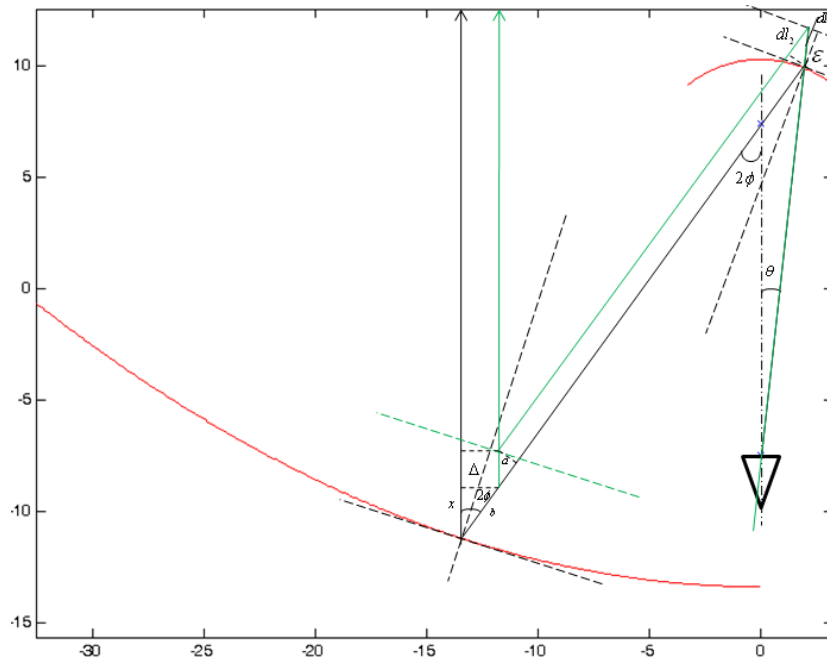


Fig. 5 Optical path of Gregory antenna.

Table 1 The Compensation Algorithm for Cassegrain Gregory Antenna

Antenna type	Cassegrain	Gregory
$\varepsilon (\Delta)$	$\varepsilon = \frac{\cos(\phi)}{\cos\left(\frac{2\phi+\theta}{2}\right)} \Delta$	$\varepsilon = \frac{\cos(\phi)}{\cos\left(\frac{2\phi-\theta}{2}\right)} \Delta$
dl_1	$\frac{-\varepsilon}{\cos\left(\frac{2\phi+\theta}{2}\right)}$	$\frac{\varepsilon}{\cos\left(\frac{2\phi-\theta}{2}\right)}$
dl_2	$\frac{-\varepsilon \cos(2\phi+\theta)}{\cos\left(\frac{2\phi+\theta}{2}\right)}$	$\frac{\varepsilon \cos(2\phi-\theta)}{\cos\left(\frac{2\phi-\theta}{2}\right)}$
dl'_2	$\frac{\Delta}{\cos(\theta)} - 2\varepsilon \cos\left(\frac{2\phi+\theta}{2}\right) \tan(\phi)$	$\frac{-\Delta}{\cos(\theta)} + 2\varepsilon \cos\left(\frac{2\phi-\theta}{2}\right) \tan(\phi)$
dl_3	$2\varepsilon \sin\left(\frac{2\phi+\theta}{2}\right) \tan(\phi) + \Delta \frac{\cos(2\phi)}{\cos(\phi)}$	$-2\varepsilon \sin\left(\frac{2\phi-\theta}{2}\right) \tan(\phi) - \Delta \frac{\cos(2\phi)}{\cos(\phi)}$

Notes: Δ -main reflector deformation; ε -sub-reflector compensation.

deformation. Figure 7 shows the TM65 telescope Finite Element Method (FEM) main reflector deformation model at 5-degree elevation (up image) and the corresponding sub-reflector deformation compensation (down image).

To obtain high efficiency, low side lobe and low noise performance, modified dish shapes are usually used in modern antenna designs. For example, the main reflector is a modified paraboloid, and the reflection surface is a modified hyperboloid or ellipsoid. In this case, The constraint condition is that the total length of the optical path remains unchanged. When realizing by programs, the input parameters are the main reflector deformation and the certain position. The output parameters are the adjustment quantity and the corresponding position of the sub-reflector. The iterative algorithm is used in the calculation process, where the calculation of the ray path is firstly from the feed to the sub-reflector, then from the sub-reflector to the main reflector, and finally from the main reflector to the aperture surface. The total length of the three sections should be unchanged. The criterion is that the difference of the optical path is less than a certain threshold. Finally, the amount of deformation of the sub-reflector and corresponding position are given.

2.2 Sub-reflector Position and Aperture Phase Simulation

The change in the position and attitude of the sub-reflector can result in a change in the phase of the aperture and vice versa in theory. Therefore, by detecting the phase distribution of the aperture plane, the position information of the sub-reflector can also be obtained.

To separate the position offsets of the sub-reflector, the primary focus, Cassegrain and Gregory sub-reflector offset method are used respectively. Herein, the primary focus offset is discussed as an example to illustrate the algorithm of phase calculation and aperture plane deviation. In the following formula, ΔX , ΔY , ΔZ are the phase of each point on the aperture plane. δ_X , δ_Y , δ_Z are the focus positions. θ is the angle between the ray from the primary focus to the main reflector, and the optical axis. Φ is the angle of

the point in the aperture plane referenced by the horizontal direction. r is the radius corresponding to this point on the surface, f is the focal length.

$$\begin{aligned} \delta_X &= \frac{2\pi}{\lambda} \sin(\theta) \cos \phi \cdot \Delta X \\ &= \frac{2\pi}{\lambda} \cdot \frac{r/f}{1 + (r/2f)^2} \cos \phi \cdot \Delta X, \end{aligned} \quad (11)$$

$$\begin{aligned} \delta_Y &= \frac{2\pi}{\lambda} \sin(\theta) \sin \phi \cdot \Delta Y \\ &= \frac{2\pi}{\lambda} \cdot \frac{r/f}{1 + (r/2f)^2} \sin \phi \cdot \Delta Y, \end{aligned} \quad (12)$$

$$\begin{aligned} \delta_Z &= \frac{2\pi}{\lambda} (1 - \cos \theta) \Delta Z \\ &= \frac{2\pi}{\lambda} \cdot \frac{2(r/2f)^2}{1 + (r/2f)^2} \Delta Z. \end{aligned} \quad (13)$$

Table 2 shows the relationship between the aperture phase and feed or sub-reflector offsets of the three antenna structures, where θ_f is the angle between the ray from the sub-reflector to the feed and the optical axis.

2.3 The Position Measurement of the Sub-reflector Based on the Aperture Phase

To obtain the optimum position of the sub-reflector, the traditional amplitude scanning method or the aperture phase fitting method can be applied. The implementation of the amplitude scanning method is based on an adjustable sub-reflector. By setting several positions in a certain direction (such as the Z direction of the sub-reflector), we can scan the antenna to obtain the beam amplitude corresponding to the each position. Then, the quadratic fitting of the beams' peaks is performed and the optimal Z -direction position is obtained. This method has been fully introduced on Tianma radio telescope and the aperture efficiency improvement is remarkable.

The aperture phase fitting method firstly requires another antenna for interferometry. The measurement antenna scans around the target source to get the two-dimensional pattern, and the reference antenna always

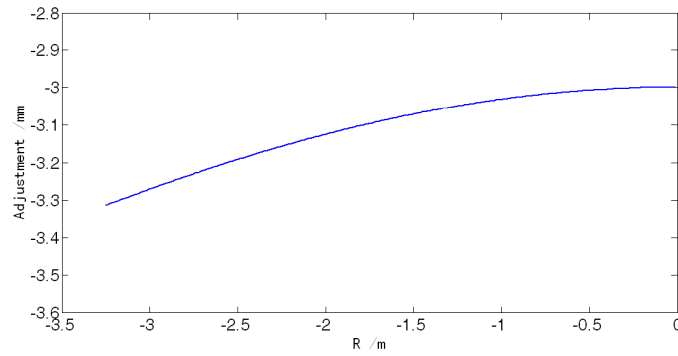


Fig. 6 The sub-reflector compensation for -3 mm deviation on main reflector.

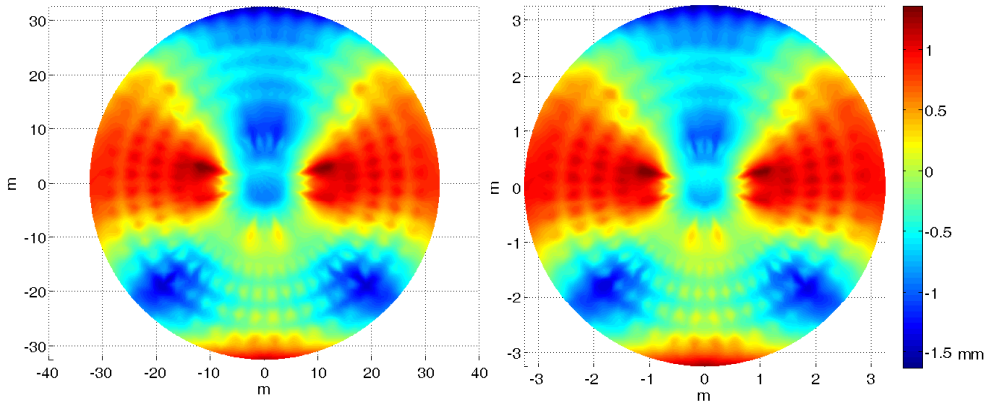


Fig. 7 Main reflector deformation (Left) and the sub-reflector compensation (Right).

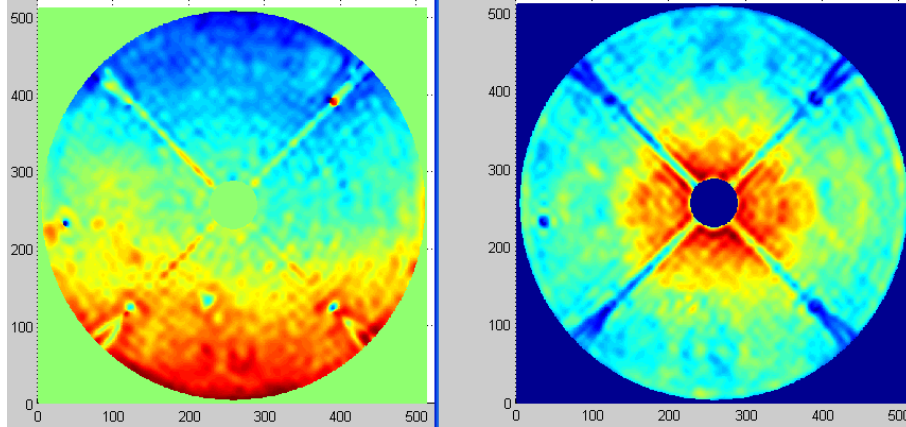


Fig. 8 Aperture phase (Left: before trend taken; Right: after trend taken).

points to the target source. The amplitude and phase of the two-dimensional far-field pattern can be obtained by the cross-correlation. Herein, the aperture phase is obtained based on the Fourier transform relationship between the aperture field and the far field. This method is also called a microwave holographic measurement.

Figure 8 is the aperture phase obtained by a microwave holographic measurement. From the phase distributions, the primary focal length of X , Y and Z directions can be solved according to the above model in Table 2. Once

the sub-reflector model is used, the sub-reflector offset can also be solved. For the same aperture phase offset, the calculated sub-reflector offset is larger than that of the primary focus, as listed in Table 3.

After obtaining the phase of the aperture at each elevation, the least squares fitting model described in Table 2 can be adopted to obtain the attitude information of the sub-reflector. It is worth mentioning that the trend change of the aperture phase is mainly caused by the sub-reflector attitude. Figure 9 shows the X , Y and Z positions for

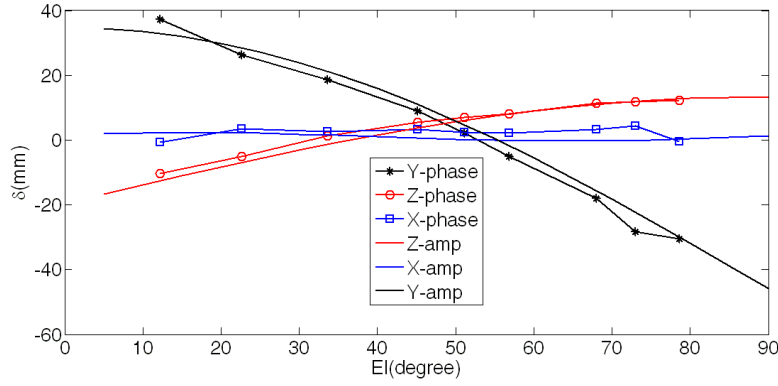


Fig. 9 Sub-reflector position model derived from aperture phase method (-phase) and traditional amplitude method (-amp) respectively.

Table 2 Aperture Phase and Feed or Sub-reflector Offsets Relationship

Offset type	primary focus mode	Cassegrain or Gregory mode
Feed offset in Z δ_Z	$\delta_Z = \frac{2\pi}{\lambda} (1 - \cos \theta) \Delta Z$	$\delta_Z = \frac{2\pi}{\lambda} (1 - \cos \theta_f) \Delta Z$
Feed offset in X δ_X	$\delta_X = \frac{2\pi}{\lambda} \sin \theta \cos \phi \cdot \Delta X$	$\delta_X = \frac{2\pi}{\lambda} \sin \theta_f \cos \phi \cdot \Delta X$
Sub-reflector offset in Z δ_Z	—	$\delta_Z = \frac{2\pi}{\lambda} [(1 - \cos \theta) + (1 - \cos \theta_f)] \Delta Z$
Sub-reflector offset in X δ_X	—	$\delta_X = \frac{2\pi}{\lambda} (\sin \theta - \sin \theta_f) \cdot \Delta X$

Table 3 Primary Focus and Cassegrain Sub-reflector Offset Derived from the Same Aperture Phase

	X	Y	Z
Primary focus	-0.534	-4.180	0.098
Cassegrain sub-reflector	-0.655	-5.165	-0.100

the sub-reflector of Tianma radio telescope measured by aperture phase, which agree well with the results from the traditional amplitude scanning method (Sun et al. 2016). During the measurement of the TM65 aperture phase, the reference antenna Sheshan 25 m radio telescope was adopted, which is about 6 kilometers far away from the measured radio telescope. The observation is just a VLBI (Very Long Baseline Interferometry). The sub-reflector is kept fixed during the measurement. The trend variation of the aperture phase is applied to solve the position of the sub-reflector.

The successful practice of this method shows that the aperture phase method can be used to diagnose the optimum position of the sub-reflector in the radio telescopes. A VLBI observation can be organized, and after the data processing, the position offsets of the sub-reflector can be given in X, Y and Z directions.

3 SUMMARY

This paper focuses on the deformable and position adjustable active sub-reflector. The surface adjustment algorithm based on the ray tracing method is derived along with

simulation results. The paper also gives the relationship between the sub-reflector offsets and the aperture phase. The sub-reflector position model is obtained on TM65 radio telescope by the aperture phase method, which agrees well with that from the traditional method. This method provides a novel way to detect the sub-reflector position, which is not easy to be measured for a radio telescope with a fixed sub-reflector.

Acknowledgements This work was supported by the National Key R&D Program of China (No. 2018YFA0404702), the National Natural Science Foundation of China (Grant Nos. A030802 and U1631114) and CAS Key Technology Talent Program.

References

Antebi, J., Zarghamee, M. S., Kan, F. W., et al. 1994, IEEE Antennas and Propagation Magazine, 36, 19
 Cheimets, P. 1994, in Society of Photo-Optical Instrumentation Engineers (SPIE) Conference Series, 2200, Proc. SPIE, ed. J. B. Breckinridge, 347
 Gasho, V. L., Radford, S. J. E., & Kingsley, J. S. 2003, in Society of Photo-Optical Instrumentation Engineers (SPIE) Conference Series, 4837, Proc. SPIE, eds. J. M. Oschmann & L. M. Stepp, 430
 Hoppe, D. J. 2001, Interplanetary Network Progress Report, 145,

- Katow, M. S., Khan, I., & Williams, W. F. 1983, Telecommunications and Data Acquisition Progress Report, 75, 65
- Lawson, P. R., & Yen, J. L. 1988, IEEE Transactions on Antennas and Propagation, 36, 1343
- Leng, G. J., & Wang, W. and Duan, B. Y. e. a. 2011, Systems Engineering and Electronics (in Chinese), 33, 996
- Nikolic, B., Prestage, R. M., Balser, D. S., Chandler, C. J., & Hills, R. E. 2007, A&A, 465, 685
- Sun, Z.-X., Wang, J.-Q., & Chen, L. 2016, RAA (Research in Astronomy and Astrophysics), 16, 119
- Viskum, H. H., & Klooster, K. V. & Zocchi, F. 2013, International Communications Satellite Systems Conference and Exhibit, 2003, 2221
- von Hoerner, S., & Wong, W.-Y. 1979, IEEE Transactions on Antennas and Propagation, 27, 720
- Wang, C. S., & Li, J. J. 2014, Electro-Mechanical Engineering (in Chinese), 29, 5
- Wang, J., Yu, L., Zhao, R., et al. 2014, Scientia Sinica Physica, Mechanica & Astronomica, 44, 1232
- Wu, T. K. 2015, Microwave & Optical Technology Letters, 14, 221
- Xu, S., Rahmat-Samii, Y., & Imbriale, W. A. 2009, IEEE Transactions on Antennas and Propagation, 57, 364
- Zuo, Y. X., Li, Y., Sun, J. X., et al. 2011, Acta Astronomica Sinica, 52, 152